Characteristics of Space and Surface Waves in a Multilayered Structure

ARUN K. BHATTACHARYYA, MEMBER, IEEE

Abstract—**Characteristics of space and surface-wave fields produced by an electromagnetic source in a multilayered structure are explored. Using the integral transformation technique it is shown that the space and surface-wave modes are orthogonal along the longitudinal direction with respect to an appropriate weighting function. It is demonstrated that these properties, together with reciprocity, can be utilized to determine the amplitudes of various surface-wave modes produced by an arbitrarily shaped source. Numerical results for the space and surface-wave power for a circular patch antenna are presented. The study may find application for millimeter-wave printed antennas where the surface waves will play an important role in determining the radiation and impedance characteristics.**

I. Introduction

MICROSTRIP ANTENNAS are popular because of their low profile and light weight [1]. They have, however, several disadvantages, one of which is lower directive gain. The directive gain can be increased by etching a patch on a multilayered substrate [2]–[4] and/or by increasing the substrate thickness. However, if the total thickness of the substrate increases, the structure starts exciting stronger surface-wave modes, which do not contribute to the radiated field. The surface-wave modes therefore reduce the radiation efficiency of the patch antenna. In order to estimate the radiation efficiency of a patch, a knowledge of the space and surface-wave modes is very important.

Radiation characteristics of an electromagnetic (EM) source placed inside a multilayered structure are reported by a number of investigators [2]–[5]. In [2], Jackson and Alexopoulos determined the space waves (far fields) of a Hertzian dipole placed inside a two-layered structure. Other papers [3]–[5] deal with the similar radiation problems. In [6], Pozar reported a moment method solution for the radiation characteristics of printed dipole and patch antennas. Results for the resonant resistance, bandwidth, surface-wave loss and dielectric loss are presented in that paper.

In the present investigation, characteristics of the space and surface waves in a multilayered structure are explored. A Hertzian magnetic dipole is considered to be the source of the various space and surface waves. The space and surface waves are determined by employing the integral transformation technique [7]. It is found that the surface-wave field distribution along the longitudinal direction (z) follows the source free transmission line equation. This characteristic leads to some more important properties, such as uniqueness (field distribution is independent of the source location) and orthogonality along z. A similar orthogonal relationship was shown in [11] using reciprocity theorem. It is demonstrated how the above properties can be utilized to determine the surface-wave fields due to an arbitrarily shaped source. Finally, numerical results for the space and surface-wave power from a circular patch on an electrically thick substrate are presented. Radiation efficiency for one-, two-, and three-layered structure are also shown. This study will be applicable to determine the space and surface-wave components produced by a printed antenna and the radiation efficiency, especially in the millimeter-wave frequency range.

Manuscript received February 17, 1989. This work was supported by the Natural Science and Engineering Research Council of Canada.

The author is with the Department of Electrical Engineering, University of Saskatchewan, Saskatoon, Canada S7N 0W0.

IEEE Log Number 9036294.

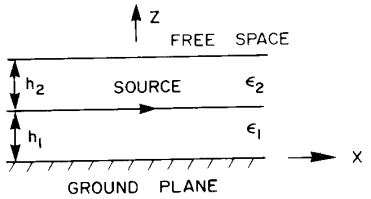

Fig. 1. Configuration of a grounded multilayered structure.

II. Fields of a Hertzian Dipole in a Multilayered Structure

Consider a multilayered structure shown in Fig. 1. An x-directed Hertzian magnetic dipole is placed inside the structure. This source can be expressed as a surface current placed at $z = h_1$ given by (a time dependence of $e^{j\omega t}$ is assumed):

$$\vec{M} = \hat{x} I_0 \delta(x)\delta(y). \tag{1}$$

The electromagnetic fields produced by the above surface current can be determined once the longitudinal components of the electric and magnetic displacement vectors are known [8]. The above quantities can be obtained by employing the integral transformation technique [7]. The expression for the longitudinal component of the electric displacement vector is obtained as

$$D_z(x, y, z) = \int_{-\infty}^{\infty}\int v(k_x, k_y, z) e^{-jk_x x - jk_y y}\, dk_x\, dk_y \tag{2}$$

where v is the line voltage (at z) of the equivalent transmission line circuit (Fig. 2) for the transverse magnetic (TM) mode (TM to z) in the transformed domain. The characteristic ad-

0018-926X/90/0800-1231$01.00

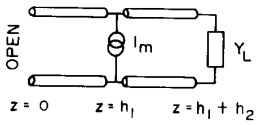

Fig. 2. Transmission line equivalent circuit of a multilayered structure in the spectral domain.

mittances of transmission line sections can be obtained from the equation:

$$y_{0i} = jk_{iz}/\epsilon_i, \qquad i = 1, 2 \cdots$$
$$\text{with } k_{iz}^2 = k_i^2 - k_x^2 - k_y^2, \quad (3)$$

where k_i is the propagation constant of the EM wave in the ith layer and ϵ_i is the permittivity of the above medium. For a two-layered structure, $v(k_x, k_y, z)$ is obtained as

$$v(k_x, k_y, z) = I_m f_m(k_x, k_y, z)/y_{\text{in}}^{\text{TM}} \quad (4)$$

with

$$f_m(k_x, k_y, z)$$
$$= \cos(k_{1z}(h_1 + z))/\cos(k_{1z}h_1), \qquad \text{for } z < h_1 \quad (5a)$$
$$= \frac{y_{02}\cos(k_{2z}(h_2 - z)) + jy_L \sin(k_{2z}(h_z - z))}{y_{02}\cos(k_{2z}h_2) + jy_L \sin(k_{2z}h_2)},$$
$$\text{for } h_1 < z < h_1 + h_2 \quad (5b)$$
$$= \frac{y_{02}e^{-jk_{0z}(z-h_2)}}{y_{02}\cos(k_{2z}h_2) + jy_L \sin(k_{2z}h_2)},$$
$$\text{for } z > h_2 + h_1 \quad (5c)$$

where y_L is the characteristic admittance of the equivalent transmission line due to free space and $y_{\text{in}}^{\text{TM}}$ is the input admittance seen by the source I_m. Expressions for the source current I_m and the admittance $y_{\text{in}}^{\text{TM}}$ are [9]

$$I_m = jk_y I_0/4\pi^2 \quad (6)$$

and

$$y_{\text{in}}^{\text{TM}} = jy_{01}\tan(k_{1z}h_1) + y_{02}\frac{y_L + jy_{02}\tan(k_{2z}h_2)}{y_{02} + jy_L \tan(k_{2z}h_z)}$$
$$\text{(for two-layered structure).} \quad (7)$$

It can be noted that both $f_m(k_x, k_y, z)$ and $y_{\text{in}}^{\text{TM}}$ are functions of $k_x^2 + k_y^2$ $(= k_\rho^2)$. Therefore, by substituting $k_x = k_\rho \cos\alpha$, $k_y = k_\rho \sin\alpha$, $x = \rho\cos\phi$ and $y = \rho\sin\phi$, we can express D_z as

$$D_z = \frac{-I_0}{2\pi}\sin\phi \int_0^\infty \frac{f_m(k_\rho, z)}{y_{\text{in}}^{\text{TM}}(k_\rho)} J_1(k_\rho\rho)k_\rho^2 dk_\rho \quad (8)$$

were $J_1(\cdot)$ represents the Bessel function of order one.

Following a very similar procedure, we obtain an expression for B_z as follows:

$$B_z = \frac{I_0\cos\phi}{2\pi j\omega}\int_0^\infty \mu_i \frac{J_1(k_\rho\rho)k_\rho^2}{y_{\text{in}}^{\text{TE}}(k_\rho)k_{iz}^2}\frac{\partial f_e(k_\rho, z)}{\partial z} dk_\rho \quad (9)$$

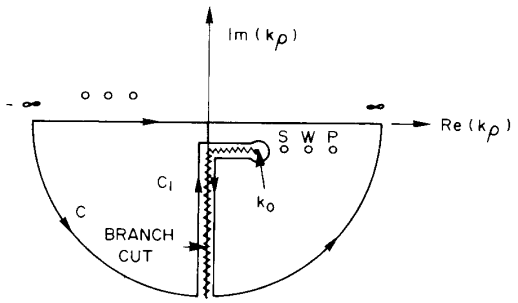

Fig. 3. Deformed contour of the infinite integral in (12).

where f_e is the line voltage in the transverse electric (TE) mode transmission line equivalent circuit and $y_{\text{in}}^{\text{TE}}(k_\rho)$ is the input admittance of the circuit at the source location. These quantities assume similar expressions as in f_m and $y_{\text{in}}^{\text{TM}}$, given in (5) and (7), respectively. However, the transmission line parameters should correspond to that of the TE mode. The characteristic admittance of the TE mode transmission line equivalent circuit should be used as [7]

$$y_{0i} = -j\mu_i/k_{iz} \quad (10)$$

where μ_i is the permeability of the ith layer.

In this section we derived the expressions for D_z and B_z. All other components of the EM fields can be determined from D_z and B_z using the procedure given in [9]. Expressions for D_z and B_z in (8) and (9) include the space and surface-wave fields. These fields will be expressed separately in the following section.

A. Space and Surface-Wave Fields

In order to extract the space and surface-wave fields from the total field, we write the expression for D_z in a slightly modified form. The functions f_m and $y_{\text{in}}^{\text{TM}}$ even with respect to k_ρ, and since $H_1^{(2)}(-x)$ is equal to $H_1^{(1)}(x)$ [10], D_z can be expressed as

$$D_z = \frac{-I_0}{4\pi}\sin\phi\int_{-\infty}^{\infty}\frac{f_m(k_\rho, z)}{y_{\text{in}}^{\text{TM}}(k_\rho)}H_1^{(2)}(k_\rho\rho)k_\rho^2 dk_\rho. \quad (11)$$

In the above expression $H_1^{(2)}(\cdot)$ represents the Hankel function of the second kind. Note that the function $y_{\text{in}}^{\text{TM}}(k_\rho)$ has two branch points [11] at $k_\rho = \pm k_0$, where k_0 is the propagation constant in free space, considered to be a complex number in order to make the branch points lie off the real k_ρ axis.

The integration in (11) can be performed along an alternate contour c as shown in Fig. 3. Such a contour was chosen in order to make the integrand analytic along the contour. We have the option of selecting any branch cut joining the branch point and the periphery of the semicircle in Fig. 3. However, this particular branch cut (Fig. 3) is selected to facilitate numerical computation of the real part of the integral.

It can be noted that the deformed contour captures some poles of the integrand which are the zeros of $y_{\text{in}}^{\text{TM}}(k_\rho)$. From the principle of contour integration, the integration in (11) can

be written as

$$D_z = \frac{-I_0}{4\pi} \sin\phi \int_c \frac{f_m(k_\rho, z)}{y_{\text{in}}(k_\rho)} H_1^{(2)}(k_\rho \rho) k_\rho^2 \, dk_\rho + \frac{I_0}{4\pi} \sin\phi \, 2\pi j \sum_n \text{residue at } k_{\rho 0}^{\text{TM}(n)} \quad (12)$$

where $k_{\rho 0}^{\text{TM}(n)}$ is the nth zero of $y_{\text{in}}^{\text{TM}}(k_\rho)$.

The numerical value of $H_1^{(2)}(k_\rho \rho)$ is zero on the circular segments of the contour c, so those parts do not contribute to the integral. Moreover, the real part of k_ρ is always less than that of k_0 on c_1, so the z-dependence of the integrand in (12) represents a wave propagation in $z(z > h_1 + h_2)$. The first term, therefore, corresponds to the space wave generated by the source. On the other hand, the z-dependence of each residue is an exponentially decaying function (since $\text{Im}(k_z) < 0$) along z, when $z > h_1 + h_2$. The last term in (12) represents the surface-wave fields. The number of surface-wave modes is equal to the number of zeros of y_{in}. The surface-wave field for the nth surface-wave mode is obtained as

$$D_{z,s}^{(n)} = \frac{jI0}{2} \sin\phi \, f_m(k_{\rho 0}^{\text{TM}(n)}, z) \, H_1^{(2)}(k_{\rho 0}^{\text{TM}(n)} \rho)(k_{\rho 0}^{\text{TM}(n)})^2 \Big/ \frac{\partial y_{\text{in}}^{\text{TM}}}{\partial k_\rho} \, (\text{at } k_\rho = k_{\rho 0}^{\text{TM}(n)}). \quad (13)$$

The surface-wave field for the TE modes can be determined from B_z. The nth surface-wave field is derived as

$$B_{z,s}^{(n)} = \frac{\mu_i I_0}{2\omega} \cos\phi \frac{\partial f_e}{\partial z} \, H_1^{(2)}(k_{\rho 0}^{\text{TE}(n)} \rho)(k_{\rho 0}^{\text{TE}(n)})^2 / k_{iz}^2 \frac{\partial y_{\text{in}}^{\text{TE}}}{\partial k_\rho} \, (\text{at } k_\rho = k_{\rho 0}^{\text{TE}(n)}) \quad (14)$$

where $k_{\rho 0}^{\text{TE}(n)}$ is the nth zero of $y_{\text{in}}^{\text{TE}}(k_\rho)$.

The space and surface-wave fields of a dipole source are determined. Important characteristics of the surface-wave field components will be obtained in the following section.

III. Characteristics of the Space and Surface-Wave Fields

The space and surface-wave fields exhibit some important characteristics. These are discussed in this section.

A. z-dependence of the Surface-Wave Fields Follows the Source-Free Transmission Line Equations

The above property of $D_{z,s}$ can be proved in the following way. We know that $v(k_x, k_y, z)$ in (2) follows the equation [7]:

$$\frac{\partial^2 v}{\partial z^2} + (k_i^2 - k_\rho^2) v = \frac{1}{\epsilon} \frac{\partial \epsilon}{\partial z} \frac{\partial v}{\partial z} - \epsilon I_m \delta(z - h_1). \quad (15)$$

Combining (4) and, (15), we obtain

$$\frac{\partial^2 f_m}{\partial z^2} + (k_i^2 - k_\rho^2) f_m = \frac{1}{\epsilon} \frac{\partial \epsilon}{\partial z} \frac{\partial f_m}{\partial z} - \epsilon y_{\text{in}}^{\text{TM}} \delta(z - h_1). \quad (16)$$

when $k_\rho = k_{\rho 0}^{\text{TM}(n)}$, the last term of the right-hand side becomes equal to zero, since $y_{\text{in}}(k_{\rho 0}^{\text{TM}(n)}) = 0$. $f_m(k_{\rho 0}^{\text{TM}(n)}, z)$ gives the z-dependence of the nth (TM) surface-wave mode and hence,

$$\frac{\partial^2 f_m(k_{\rho 0}^{\text{TM}(n)}, z)}{\partial z^2} + (k_i^2 - k_{\rho 0}^{\text{TM}(n)2}) f_m(k_{\rho 0}^{\text{TM}(n)}, z) = \frac{1}{\epsilon} \frac{\partial \epsilon}{\partial z} \frac{\partial f_m(k_{\rho 0}^{\text{TM}(n)}, z)}{\partial z}. \quad (17)$$

In a similar manner it can be shown that $g_e = \mu(\partial f_e / \partial z)/k_z^2$ also follows a similar equation as f_m, except that on the right-hand side of (17), ϵ should be replaced by μ.

It is to be noted that in the right of (16) and (17), the term $\partial\epsilon/\partial z$ is not equal to zero, in general. In the case of a layered media, this term is equal to a series of Dirac-delta functions. In the case of inhomogeneous dielectric (inhomogenity along z), it will be a continuous function except at the air-dielectric interface.

B. Surface-Wave Modes of the same Type (either TE or TM) are Orthogonal Along the z-direction

Suppose f_{m1} and f_{m2} represent the z-variation of two TM surface-wave mode fields. Each satisfies (17). With some algebraic manipulation, it can be shown that the following relation holds:

$$\frac{\partial X}{\partial z} + (k_{\rho 0}^{\text{TM}(2)^2} - k_{\rho 0}^{\text{TM}(1)^2}) f_{m1} f_{m2} - \frac{1}{\epsilon} \frac{\partial \epsilon}{\partial z} X = 0 \quad (18)$$

with

$$X = f_{m2} \frac{\partial f_{m1}}{\partial z} - f_{m1} \frac{\partial f_{m2}}{\partial Z}. \quad (19)$$

Multiplying (18) by $1/\epsilon$, we have

$$\frac{\partial}{\partial z}(X/\epsilon) + (k_{\rho 0}^{\text{TM}(2)^2} - k_{\rho 0}^{\text{TM}(1)^2}) f_{m1} f_{m2}/\epsilon = 0. \quad (20)$$

Integrating (20) with respect to z in the range $0 < z < \infty$, we have

$$\int_Z f_{m1}(k_{\rho 0}^{\text{TM}(1)}, z) f_{m2}(k_{\rho 0}^{\text{TM}(2)}, z)/\epsilon \, dz = 0, \quad (21)$$

since $X = 0$ at $z = 0$ and $z \to \infty$. The above orthogonal relationship is equivalent to the following relation:

$$\int_z E_{z,s}^{(1)} \cdot H_{\phi,s}^{(2)} \, dz \quad (22)$$

which indicates that the mutual reaction between two surface modes is zero. This proves the orthogonal characteristics of $f_m/\sqrt{\epsilon}(z)$. The TE surface-wave modes will also be orthogonal to each other, since they follow a similar equation. Equation (21) shows that $D_{z,s}^{(n)}/\sqrt{\epsilon}(z)$ are an orthogonal set of functions z at a given ρ. Similarly, $B_{z,s}^{(n)}/\sqrt{\mu}(z)$ will also form a set of orthogonal functions of z. In Fig. 4, two different (TM and TE) surface-wave mode fields are plotted against z.

It can also be shown that the z-dependence of a surface-wave field is unique and does not depend on the location of the source. This is due to the fact that the eigenfunctions for the surface-wave modes are the solutions of the source-free second-order differential equation (17).

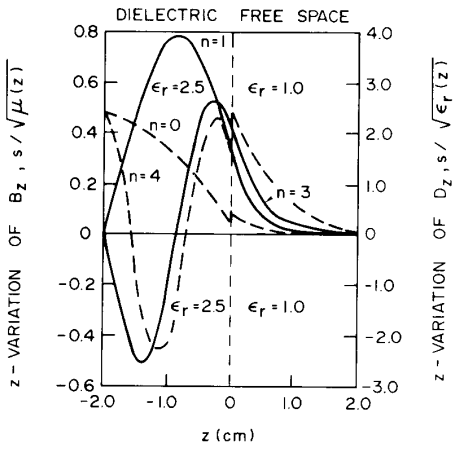

Fig. 4. Variation of the TM surface-wave fields along z for two modes in a grounded dielectric structure. - - - - TM surface-waves versus z, —— TE surface-waves versus z. ($\epsilon_r = 2.5$, $h = 2$ cm, $f = 15$ GHz.)

C. Space and Surface-Wave Fields are Orthogonal Along the z-Direction

The space wave field component, $D_{z,r}$, has been expressed in terms of a contour integral in (12), which is given by

$$D_{z,r} = \frac{-I_0}{4\pi} \sin\phi \int_{c_1} \frac{f_m(k_\rho, z)}{y_{\text{in}}} H_1^{(2)}(k_\rho \rho) k_\rho^2 \, dk_\rho \quad (23)$$

where c_1 is the contour around the branch cut shown in Fig. 3. The surface wave field, $D_{z,s}^{(n)}$, for the TM_n mode can be written as

$$D_{z,s}^{(n)} = A(k_{\rho 0}^{\text{TM}(n)}) \sin\phi \, f_m(k_{\rho 0}^{\text{TM}(n)}, z) \quad (24)$$

where $f_m(k_\rho, z)$ and $f_m(k_{\rho 0}^{\text{TM}(n)}, z)$ are the solutions of (16) and (17), respectively. Multiplying (16) by $f_m(k_{\rho 0}^{\text{TM}(n)}, z)$ and (17) by $f_m(k_\rho, z)$ and then subtracting, we obtain:

$$\frac{\partial}{\partial z}\left(\frac{W}{\epsilon}\right) + (k_{\rho 0}^{\text{TM}(n)^2} - k_\rho^2) \frac{f_m(k_\rho, z) f_m(k_{\rho 0}^{\text{TM}(n)}, z)}{\epsilon} = -y_{\text{in}}^{\text{TM}}(k_\rho)\delta(z - h_1) f_m(k_{\rho 0}^{\text{TM}(n)}, z) \quad (25)$$

where

$$W = f_m(k_{\rho 0}^{\text{TM}(n)}, z) \frac{\partial f_m(k_\rho, z)}{\partial z} - f_m(k_\rho, z) \frac{\partial f_m(k_{\rho 0}^{\text{TM}(n)}, z)}{\partial z}.$$

Integrating (25) with respect to z in the interval 0 to ∞, and rearranging the equation, we obtain

$$\int_z \frac{1}{\epsilon} f_m(k_{\rho 0}^{(n)}, z) f_m(k_\rho, z) \, dz = \frac{y_{\text{in}}^{\text{TM}}(k_\rho)}{(k_\rho^2 - k_{\rho 0}^{\text{TM}(n)2})} f_m(k_{\rho 0}^{\text{TM}(n)}, h_1). \quad (26a)$$

In deriving (26a), we used the relation $W(z = 0) = W(z = \infty) = 0$, which is true. Now consider the following integral:

$$I = \int_z \frac{1}{\epsilon} \cdot D_{z,s} \cdot D_{z,r} \, dz. \quad (26b)$$

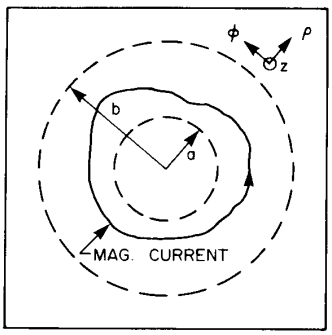

Fig. 5. An arbitrarily shaped magnetic current on a multilayered structure.

Combining (23), (24), (25) and (26) it can be shown that

$$I = \frac{I_0 A(k_{\rho 0}^{\text{TM}(n)}) \sin^2\phi}{4\pi} \int_{c_1} \frac{f_m(k_{\rho 0}^{\text{TM}(n)}, h_1)}{(k_{\rho 0}^{\text{TM}(n)2} - k_\rho^2)} H_1^{(2)}(k_\rho \rho) k_\rho^2 \, dk_\rho. \quad (27)$$

The integrand in (27) does not have any branch point or pole inside the contour c_1, and therefore, the integral vanishes. This proves the orthogonality of the space and the surface waves in z.

IV. Application to Patch Antennas

The orthogonal property of the space and surface-wave modes can be utilized to determine the amplitude of the surface-wave modes produced by an arbitrary source in a multilayered structure. An equivalent magnetic current on the radiating edge of a microstrip antenna is an example of a source in a layered structure. Since, depending on the application, a microstrip patch can be of any shape, therefore its equivalent aperture source will also follow the structural geometry. In the following example, we shall consider an arbitrarily oriented magnetic current source in a multilayered structure and determine the surface-wave modes produced by it.

The source under consideration is shown in Fig. 5. Consider two concentric cylinders of radii a and b, respectively ($b > a$), where the source lies inside the region between the two cylinders. First, we shall determine the TM surface-wave modes generated by the source. The z-directed electric displacement vector for the surface-wave mode can be expressed as

$$D_z = \sum_{mn}\sum A_{mn} H_n^{(2)}(k_{\rho 0}^{\text{TM}(m)}\rho) f_m(k_{\rho 0}^{\text{TM}(m)}, z) e^{jn\phi}, \quad \rho \geq b \quad (28a)$$

$$= \sum_{mn}\sum B_{mn} J_n(k_{\rho 0}^{\text{TM}(m)}\rho) f_m(k_{\rho 0}^{\text{TM}(m)}, z) e^{jn\phi}, \quad \rho \leq a \quad (28b)$$

where $k_{\rho 0}^{\text{TM}(m)}$ is the mth zero of $y_{\text{in}}^{\text{TM}}(k_\rho)$ and $f_m(k_{\rho 0}^{\text{TM}(m)}, z)$ is given in (5). A_{mn} and B_{mn} are unknowns to be determined. The corresponding magnetic field components can be determined using the procedure in [8], [9].

Let us consider an auxiliary source placed at $\rho = \infty$, which generates the TM_{nm} surface-wave mode only, whose EM field

is obtained from D_z^a (the superscript a stands for auxiliary) where

$$D_z^a = H_n^{(1)}(k_{\rho 0}^{\mathrm{TM}(m)}\rho) f_m(k_{\rho 0}^{\mathrm{TM}(m)}, z) e^{-jn\phi}. \quad (29)$$

From reciprocity we know [8]:

$$\oint_S (\vec{E}_a \times \vec{H}_b - \vec{E}_b \times \vec{H}_a) \cdot ds = \iiint_v (\vec{H}_a \cdot \vec{M}_b - \vec{H}_b \cdot \vec{M}_a)\, dV \quad (30)$$

where v is the volume inside the closed surface s.

In (30) we consider $(\vec{E}_b, \vec{H}_b)$ as the fields obtained from (28) and $(\vec{E}_a, \vec{H}_a)$ are the fields obtained from (29). The volume v is the entire volume formed by the annular region between the two cylinders of radius a and of radius b, shown in Fig. 5. Employing (30), we obtain

$$\frac{4\omega}{(k_{\rho 0}^{\mathrm{TM}(m)})^2}(2A_{mn} - B_{mn}) \int_z \frac{f_m^2(k_{\rho 0}^{\mathrm{TM}(m)}, z)}{\epsilon(z)}\, dz = -\iiint_v \vec{H}_a \cdot \vec{M}_b\, dV. \quad (31)$$

The orthogonal relationship among $f_m(k_{\rho 0}^{\mathrm{TM}(i)}, z)/\sqrt{\epsilon(z)}$ (for various i) and $f_m(k_\rho, z)/\sqrt{\epsilon(z)}$ was utilized to derive (31).

Now, let us choose another set of auxiliary fields whose D_z is as below:

$$\tilde{D}_z^a = H_n^{(2)}(k_{\rho 0}^{\mathrm{TM}(m)}\rho) f_m(k_{\rho 0}^{\mathrm{TM}(m)}, z) e^{-jn\phi}. \quad (32)$$

Using reciprocity, we get

$$\frac{4\omega}{(k_{\rho 0}^{\mathrm{TM}(m)})^2} B_{mn} \int_z \frac{f_m^2(k_{\rho 0}^{\mathrm{TM}(m)}, z)}{\epsilon(z)}\, dz = -\iiint_v \tilde{\vec{H}}_a \cdot \vec{M}_b\, dv. \quad (33)$$

The expression for B_{mn} can be obtained from (33). Solving (31) and (33), we obtain A_{mn} as

$$A_{mn} = \frac{-(k_{\rho 0}^{(m)})^2}{8\omega} \frac{\iiint_v (\vec{H}_a + \tilde{\vec{H}}_a) \cdot \vec{M}_b\, dv}{\int_z f_m^2(k_{\rho 0}^{(m)}, z)/\epsilon(z)\, dz}. \quad (34)$$

In order to verify the validity of the above expression, we selected

$$\vec{M}_b = E_0 h \cos n\phi\, \delta(\rho - a)\delta(z)\hat{\phi} \quad (35)$$

which is the equivalent magnetic line current on the aperture of a thin circular patch. The amplitude for the TM_{10} surface-wave mode was calculated using (34). The expression of the ϕ component of the magnetic field coincides with that obtained in [7].

The TE surface-wave fields can be determined exactly in the same way as discussed. For the TE case, the auxiliary sources should also be TE type (i.e., $D_z = 0$). The z-variation will be $g_e(k_{\rho 0}^{\mathrm{TM}(m)}, z)$, which are also orthogonal in z.

A. Circular Patch Antenna on a Thick Substrate

The above technique is employed to obtain the surface-wave powers generated by a circular patch etched on an electrically thick substrate. To obtain a generalized expression for the surface-wave power, an additional layer on the top surface of the patch was also considered (Fig. 6). The patch is assumed to be excited in the TM_1 mode (here the subscript one stands for the azimuthal variation of the field under the patch metallization). The equivalent magnetic surface current may be represented as

$$\vec{M} = E_0 \cos\phi\, \delta(\rho - a)\hat{\phi}, \qquad 0 < z < h_1 \quad (36)$$

where $E_0 \cos\phi$ is the z-directed field at $\rho = a$. Following the procedure discussed before, we obtain the amplitude of the TM_{n1} surface-wave mode as

$$A_{n1} = \frac{ja}{4} J_1'(k_{\rho 0}^{\mathrm{TM}(n)}a) E_0 \pi I_1 / I_2 \quad (37)$$

where

$$I_1 = \int_0^{h_1} f_m(k_{\rho 0}^{\mathrm{TM}(n)}, z)\, dz = \tan(k_{1z}h_1)/k_{1z} \quad (38)$$

and

$$I_2 = \int_0^\infty f_m^2(k_{\rho 0}^{\mathrm{TM}(n)}, z)/\epsilon(z)\, dz = \frac{1}{2\epsilon_0}\left[\frac{1}{\epsilon_r}\left\{h \sec^2(k_{1z}h) + \frac{\tan(k_{1z}h)}{k_{1z}}\right\} + \frac{1}{|k_{0z}|}\right]. \quad (39)$$

The total power carried out by the TM_{n1} surface-wave mode is derived as

$$P_{\mathrm{TM}}^{(n)} = \omega\pi^2 a^2 E_0^2 [J_1'(k_{\rho 0}^{\mathrm{TM}(n)}a)]^2 I_1^2 / 2I_2. \quad (40)$$

In order to obtain the TE surface-wave fields, we express B_z as

$$B_z = B_{n1} \sin\phi\, g_e(k_{\rho 0}^{\mathrm{TE}(n)}, z) H_1^{(2)}(k_{\rho 0}^{\mathrm{TE}(n)}\rho), \qquad \rho > a$$

with $g_e = \mu(\partial f_e/\partial z)/k_z^2$ where f_e has a similar expression as f_m in (5). The other field components can be generated from the electric vector potential $\vec{F} = \hat{z}F_z$, where $F_z = j\omega B_z/(k_{\rho 0}^{\mathrm{TM}(n)})^2$. Using reciprocity with an auxiliary TE surface-wave mode whose source is outside the region defined by $\rho = a$, and with a tedious but straightforward algebraic manipulation, we derive the surface wave power for the TE_{n1} mode as

$$P_{\mathrm{TE}}^{(n)} = \frac{E_0^2\pi^2}{\omega\mu_0[k_{\rho 0}^{\mathrm{TE}(n)}]^2} \frac{[J_1(k_{\rho 0}^{\mathrm{TE}(n)}a)]^2 \tan^2(k_{1z}h_1)}{\left[h \sec^2(k_{1z}h) - \frac{\tan(k_{1z}h)}{k_{1z}} + \frac{k_{1z}^2}{|k_{0z}|3}\right]}. \quad (41)$$

1) Space Wave Power: The space wave fields for the TM and TE space wave modes can be obtained from $D_{z,r}$ and

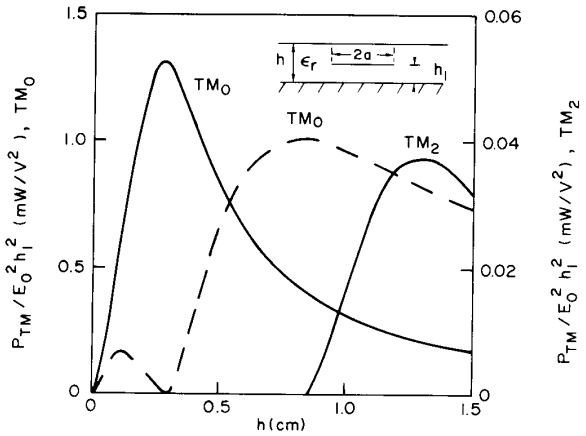

Fig. 6. Variation of normalized surface-wave power for the TM mode with dielectric thickness of a circular patch ($\epsilon_r = 2.5$, $f = 15$ GHz) —— $f_r = 15$ GHz, ---- $a = 0.5$ cm.

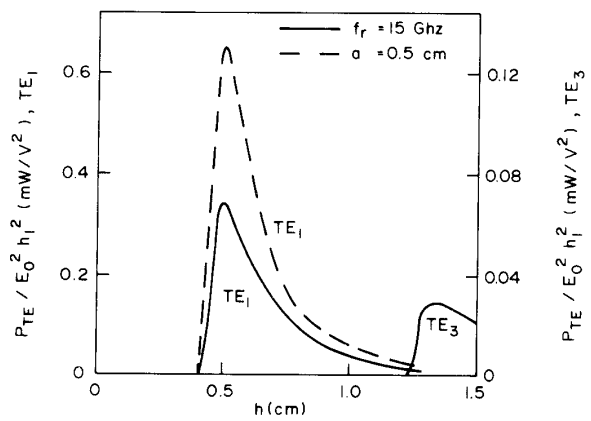

Fig. 7. Normalized surface-wave (TE) power versus the thickness of the substrate ($\epsilon_r = 2.5$, $f = 15$ GHz).

$B_{z,r}$, respectively. For a magnetic current defined in (36), expressions for $D_{z,r}$ and $B_{z,r}$ were obtained as

$$D_{z,r} = \frac{E_a \cos \phi a}{2} \int_{c_1} \int_0^{h_1} \frac{J_1'(k_\rho a) H_1^{(2)}(k_\rho \rho)}{y_{\text{in}}^{\text{TM}}} \cdot f_m(k_\rho, z) k_\rho^2 \, dh \, dk_\rho \quad (42)$$

$$B_{z,r} = -\frac{\sin \phi E_a \mu}{2j\omega} \int_{c_1} \int_0^{h_1} \frac{J_1(k_\rho a) H_1^{(2)}(k_\rho \rho)}{y_{\text{in}}^{\text{TE}} k_{1z}^2} k_\rho \frac{\partial fe}{\partial z} \, dh \, dk_\rho. \quad (43)$$

From $D_{z,r}$ and $B_{z,r}$, the ϕ-directed magnetic fields for the space waves were determined. The TM and TE space wave power were obtained by taking the inner product between the magnetic current and the magnetic field corresponding to the TM and TE waves, respectively, and integrating on the aperture surface. The real parts of the total power are contributed by the segments of the contour c_1 which are parallel to the real axis of k_ρ.

B. Numerical Results of a Circular Patch

Equations (40) and (41) were used to obtain the surface-wave (SW) power generated by a circular patch. Fig. 6 shows the variation of the normalized SW power (normalized with respect to the square of the aperture voltage of the patch at $\phi = 0°$) with the dielectric thickness. Two different dimensions of the patch were selected. The solid line indicates the characteristic of a patch whose resonant frequency is 15 GHz for the TM_{11} mode. The effective radius of the patch was obtained as $a_e \approx 0.37$ cm when $\epsilon_r = 2.5$. This was obtained from the magnetic wall model of a circular patch [1]. In (40) the power is expressed as a function of the physical radius, a, which, however, changes with the substrate thickness for a given resonant frequency. In order to estimate the physical radius for each substrate thickness the equivalent extension formula was used [1]. From Fig. 6, we note that the TM_0 surface-wave power for a resonant patch is maximum when $h/\lambda 0 \approx 0.15(\epsilon_r = 2.5)$. There are several reasons for such a characteristic of the TM_0 mode. It can be observed from (39) and (40) that for a lower substrate thickness ($h/\lambda_0 < 0.02$) the surface-wave characteristic is mostly dictated by the factor I_2 whose value is proportional to $1/|k_{0z}|$. For a small h, k_{0z} is proportional to h and, therefore, the power increases with h. For a large value of h, the surface-wave number $k_{\rho 0}^{(0)}$ approaches k_1 and the surface-wave power becomes inversely proportional to h and a decaying characteristic is observed.

The TM_2 surface-wave mode also exhibits a very similar behavior to that of the TM_0 mode. Note that the TM_0 mode exists for all substrate thicknesses while the TM_2 mode starts appearing after $h > 0.8$ cm.

The dotted curve in Fig. 6 indicates the TM_0 mode power at 15 GHz frequency for a patch with a fixed radius of 0.5 cm. The characteristics of the curve is slightly different (passes through a zero at $h \approx 0.3$ cm) than that of the patch with $a_e = 0.37$ cm. This is due to the factor $[J_1'(k_{\rho 0}^{\text{TM}(0)} a)]^2$, whose value is zero when $h \simeq 0.3$ and $a = 0.5$ cm. This means that a circular aperture of the above dimension ($a = 0.5$ cm) will not produce any surface-wave mode at 15 GHz frequency.

In Fig. 7, we have plotted the TE surface-wave power against the substrate thickness of a circular patch. Two different dimensions were taken as in Fig. 6. The TE surface-wave modes exhibit similar characteristics as the TM modes. The only difference is that the edges of the curves (rising and falling both) are sharper in the TE cases, than those of the TM cases. This is because the power in the rising edge is proportional to $|k_{0z}|^3$ (which is again proportional to Δh^3 where Δh is the incremental substrate thickness from the starting point of the TE mode); therefore the edge is sharper (recall that for the TM case, it was proportional to h). Similarly, if we expand (42) asymptotically, we can see that in the falling edge, the power is proportional to $1/h^3$, so that the decay rate is faster than that of the TM modes. The TE_1 surface-wave power is maximum when $h \approx \lambda_0/4$ for a dielectric constant of 2.5.

Fig. 8 shows the TM and TE surface-wave power of a circular patch when it is covered with a dielectric material. Here both the TE and TM surface-wave mode have similar characteristics as in Fig. 6 and 7. The total surface-wave power

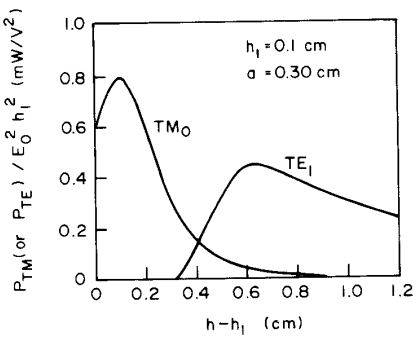

Fig. 8. Variation of the normalized surface-wave power with superstrate thickness of a circular patch ($\epsilon_r = 2.5$, $f = 15$ GHz).

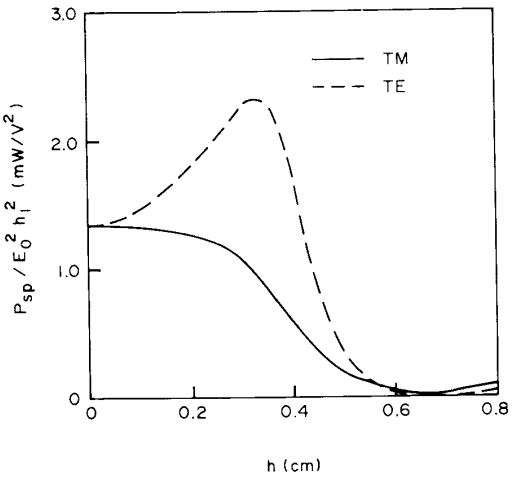

Fig. 9. Variation of the TM and TE space wave power of a circular patch with the substrate thickness ($a = 0.5$ cm, $\epsilon_r = 2.5$, $f = 15$ GHz).

(TM and TE) is minimum near the superstrate thickness of 0.4 cm.

The space wave power for the TM and TE modes of a circular patch is plotted in Fig. 9. The parameters were: $a = 0.5$ cm, $\epsilon_r = 2.5$, and $f = 15$ GHz. The TM space-wave power is found to decrease rapidly after $h = 0.3$ cm. The TE space wave power initially increases with h, then decreases quickly. The space wave power for both the modes are very small when the substrate thickness is greater than 0.6 cm. The total radiated power is maximum when the substrate thickness is near 0.3 cm.

C. Radiation Efficiency of a Multilayered Structure

The space and surface-wave power produced by a magnetic dipole were computed and the radiation efficiency was plotted in Fig. 10. The solid curve shows the radiation efficiency for a single layer structure (without superstrate) of 2 cm thick with $\epsilon_r = 2.5$. The maximum value of the radiation efficiency occurs at a frequency, when the thickness, h, is about an integral multiple of $\lambda_\epsilon/2$, where λ_ϵ is the wavelength in the dielectric. The efficiency is minimum when h is approximately equal to $\lambda_\epsilon/4$, $3\lambda_\epsilon/4$, etc.

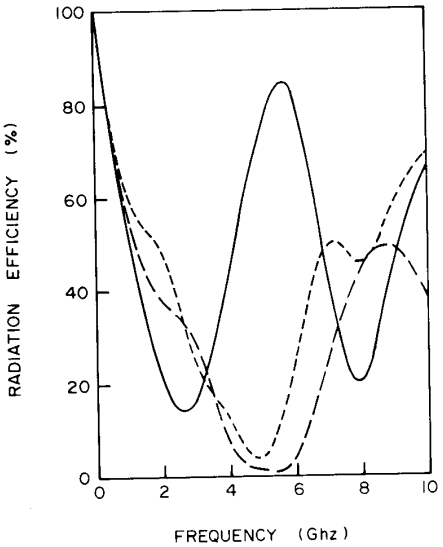

Fig. 10. Radiation efficiency for one-, two-, and three-layered structure (—— one layer, - - - - two layers, ---- three layers).

The radiation efficiency for two- and three-layered structures were also plotted in Fig. 10. In the case of a two-layered structure, h_1 and h_2 (Fig. 1) were taken as 1 cm each. The source was at the interface of two layers. In this case, the minimum value of the radiation efficiency occurs when h_1 is approximately equal to $\lambda_\epsilon/4$. For the three-layered structure, each layer has a thickness of 1 cm. The intermediate layer has a dielectric constant equal to the free space. The source is located at the interface of the first two layers. The radiation efficiency is found to vary widely with the frequency.

V. Conclusion

Important characteristics of the surface-wave modes in a multilayered grounded dielectric substrate are explored. It is shown how these characteristics can be utilized to determine the surface-wave fields of an arbitrarily shaped source. The theory was applied to a circular patch antenna on a thick substrate and with a superstrate layer over it. The above methodology is simple, straightforward, and can be applied to obtain various surface-wave modes generated by a number of structures which are used in practice. In addition, the technique can be applied to determine the surface-wave coupling between the transmission lines in a multilayered structure, or between two antennas on the same layer or between an antenna and a transmission line. The surface-wave coupling will be stronger for millimeter wave frequencies, and the present investigation may find application in that frequency range.

References

[1] I. J. Bahl and P. Bhartia, *Microstrip Antennas*. Dedham, MA: Artech House, 1980.

[2] D. R. Jackson and N. G. Alexopoulos, "Gain enhancement methods for printed circuit antennas," *IEEE Trans. Antennas Propagat.*, vol. AP-33, pp. 976-987, Sept. 1985.

[3] H. Y. Yang and N. G. Alexopoulos, "Gain enhancement methods for printed circuit antennas through multiple superstrates," *IEEE Trans. Antennas Propagat.*, vol. AP-35, pp. 860-863, July 1987.

[4] D. R. Jackson and A. A. Oliner, "A leaky-wave analysis of the high gain printed antenna configuration," *IEEE Trans. Antennas Propagat.*, vol. 36, pp. 905–910, July 1988.
[5] N. G. Alexopoulos, P. B. Katehi, and D. B. Rutledge, "Substrate optimization for integrated circuit antennas," *IEEE Trans. Microwave Theory Tech.*, vol. MTT-31, pp. 550–557, July 1983.
[6] D. M. Pozar, "Considerations for millimeter wave printed antennas," *IEEE Trans. Antennas Propagat.*, vol. AP-31, pp. 740–747, Sept. 1983.
[7] A. K. Bhattacharyya and R. Garg, "Spectral domain analysis of wall admittances for circular and annular microstrip patches and the effect of surface-waves," *IEEE Trans. Antennas Propagat.*, vol. AP-33, pp. 1067–1073, Oct. 1985.
[8] R. F. Harrington, *Time-Harmonic Electromagnetic Fields*. New York: McGraw-Hill, 1961.
[9] A. K. Bhattacharyya and R. Garg, "Effect of substrate on the efficiency of an arbitrarily shaped microstrip patch antenna," *IEEE Trans., Antennas Propagat.*, vol. AP-34, pp. 1181–1188, Oct. 1986.
[10] M. Abramowitz and I. E. Stegun, *Handbook of Mathematical Functions*, Nat. Bur. Stand., Appl. Math. Ser. 55, 1964.
[11] R. E. Collin, *Field Theory of Guided Waves*. New York: McGraw-Hill, 1960.

Arun K. Bhattacharyya (M'87), for a photograph and biography please see page 1530 of the November 1988 issue of this TRANSACTIONS.